(Received 16 September 2025, Accepted 22 October 2025, Scheduled 1 November 2025)

# A Wideband Circularly Polarized Textile-Based Microstrip Antenna for Wearable Wireless Applications

Sekhar M[1], Konkyana Lalitha Bhavani[2,*], Sanapala Umamaheswararao[2], Lokesh Raju Vysyaraju[2], Chaitanya Kumar Marpu[2], and Kotni Krishnam Raju[2]

[1]*Department of Electronics and Communication Engineering*
*Vignan's Foundation For Science, Technology and Research, Guntur, India*
[2]*Department of Electronics and Communication Engineering*
*Aditya Institute of Technology and Management, Tekkali, India*

**ABSTRACT:** This paper presents the design, fabrication, and analysis of a wideband circularly polarized wearable antenna operating in the frequency range of 2.6 GHz to 4.7 GHz. The antenna is designed on a jean's substrate with dimensions of $25 \times 30 \times 1.4\,\text{mm}^3$, having a dielectric constant of 1.7 and a loss tangent of 0.085. The proposed antenna demonstrates a gain of 2.8–3.4 dB across the operating frequency band and exhibits circular polarization in the frequency range of 3.2 GHz to 3.9 GHz. To achieve wideband performance and circular polarization, the antenna design incorporates an octagonal ring patch with a hybrid slot and stub in the partial ground plane, along with four slots in the ring patch. The antenna is fabricated, and its performance is validated through Vector Network Analyzer and anechoic chamber measurements, showing good correlation with simulated results. Specific Absorption Rate (SAR) analysis and on-body simulations are conducted to evaluate its suitability for wearable applications.

## 1. INTRODUCTION

Wearable antennas have emerged as a critical component in modern wireless communication systems, particularly for applications in wireless body area networks (WBANs), healthcare monitoring, and personal communication devices [1]. The growing demand for compact, flexible, and efficient antennas has driven significant research into innovative designs that can operate effectively in on-body environments [2]. Wearable antennas must meet stringent requirements, including flexibility, biocompatibility, and robustness to the effects of human tissue, while maintaining high performance in terms of bandwidth, gain, and radiation efficiency [3]. Recent advancements in wearable antenna design have focused on the use of flexible substrates, such as textiles, to ensure comfort and durability. Jeans fabric, in particular, has gained attention due to its low cost, flexibility, and favorable dielectric properties, making it an ideal candidate for wearable applications [4]. Additionally, the integration of wideband and circularly polarized (CP) characteristics in wearable antennas has been extensively studied to address the challenges of multipath interference and signal degradation in dynamic environments.

Wearable antennas have become a key component in modern wireless body sensor networks (WBSNs), biomedical monitoring, and communication systems, leading to extensive research in flexible, textile-based, and conformal antenna designs. Several studies have explored innovative approaches to enhance bandwidth, gain, Specific Absorption Rate (SAR) compliance, and structural flexibility of wearable antennas. Recently, various circularly polarized printed antenna techniques have been proposed, including the use of metasurface-based configurations, hybrid slots, and perturbation techniques to excite orthogonal modes with a 90° phase difference. For instance, an all-textile circularly polarized metasurface antenna demonstrated wide impedance and axial ratio bandwidths with high gain and conformal stability under bending and human body loading [5]. Similarly, U-shaped textile antennas on denim substrates achieved wide axial ratio bandwidths (2.1–3.72 GHz) and stable performance under mechanical deformation, confirming the suitability of textile materials for circularly polarized wearable designs [6, 7].

Research has demonstrated that textile-based antennas, such as those using denim, silk, neoprene, Cordura, and Kapton polyimide fabrics, offer mechanical flexibility, low dielectric constants, and ease of integration into clothing [8–11]. Some studies have focused on dual-band and ultra-wideband (UWB) designs for applications such as LoRa, BLE, Wi-Fi, and biomedical sensing, showing that the choice of substrate material and antenna topology significantly impacts performance [10–15]. Additionally, techniques like slot incorporation, artificial magnetic conductors (AMCs), metasurfaces, and electromagnetic bandgap (EBG) structures have been employed to reduce SAR values and improve radiation efficiency. For example, a wideband stub-loaded monopole antenna backed with a hexagonal EBG array achieved significant SAR reduction (0.44 W/kg) while improving gain and back radiation isolation, highlighting the importance of body decoupling techniques in wearable scenarios [16].

* Corresponding author: Lalitha Bhavani Konkyana (kvlb2003@gmail.com).

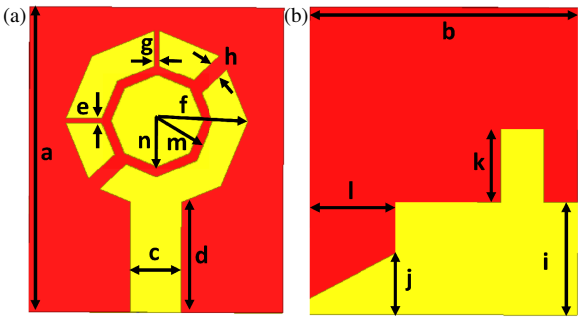


**FIGURE 1**. Proposed antenna. (a) Top view. (b) Rear view.

To ensure that wearable antennas function optimally in real-world conditions, studies have emphasized the impact of bending, conformal analysis, and human body interaction on antenna performance. The SAR compliance of various antenna designs has been evaluated using phantom models, confirming that many proposed designs meet US Federal Communications Commission (FCC) and European Union (EU) safety regulations [5, 8, 10, 13]. Conformal analysis has also been conducted on curved surfaces to validate the antennas' robustness under practical conditions [6, 14, 15]. These findings confirm that flexible substrates and optimized geometries can maintain stable impedance and radiation properties even under deformation. Additionally, research has explored the potential of wearable antennas for biomedical and defense applications, demonstrating their effectiveness in reliable on- and off-body communication [5, 7].

This paper presents the design, fabrication, and analysis of a wideband circularly polarized wearable antenna operating from 2.6 GHz to 4.7 GHz, suitable for Wi-Fi, LTE, and sub-6 GHz 5G applications. The antenna is implemented on a jeans textile substrate, ensuring flexibility and user comfort. The proposed design features an octagonal ring patch with a hybrid slot and stub in a partial ground plane, optimized for wideband performance, while four slots in the ring patch enable circular polarization between 3.2 GHz and 3.9 GHz. The antenna is fabricated and validated through $S_{11}$ measurements demonstrating good agreement with simulations. Additionally, SAR analysis, on-body simulations, and conformal evaluations are conducted to assess its performance in real-world conditions.

## 2. ANTENNA DESIGN

The design of the proposed wideband circularly polarized wearable antenna was carried out in multiple stages to achieve optimal performance in terms of bandwidth, gain, and circular polarization. Initially, an octagonal patch with a microstrip feed line and a full ground plane was implemented on a jeans substrate ($\varepsilon_r = 1.7$, $\tan\delta = 0.085$). However, this configuration resulted in a narrow bandwidth, limiting its suitability for wideband applications. To enhance the impedance bandwidth, the octagonal patch was modified into an octagonal ring patch, allowing better current distribution and impedance matching. Additionally, the full ground plane was replaced with a partial ground plane, further improving the bandwidth by increasing the effective radiation area.

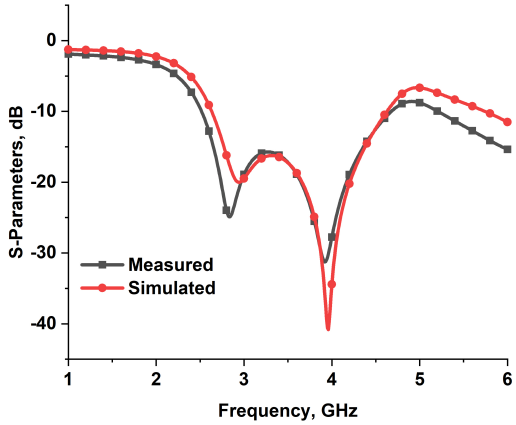


**FIGURE 2**. Return loss of wideband antenna.

To achieve additional bandwidth enhancement, an inner octagonal patch was introduced within the ring patch, and a hybrid slot along with a stub was incorporated into the partial ground plane. These modifications optimized the antenna's impedance characteristics across the 2.6–4.7 GHz frequency range. Furthermore, to enable circular polarization between 3.2 GHz and 3.9 GHz, four symmetrical slots were introduced in the ring patch, creating orthogonal current components that improved polarization purity. The final antenna design presented in Figure 1 achieved stable radiation characteristics, wide impedance bandwidth, and circular polarization, making it well-suited for wearable applications. The optimized dimensions of the antenna are presented in Table 1. The antenna has a fractional bandwidth of 57.5%, ranging from 2.6 GHz to 4.7 GHz, as shown in Figure 2. The antenna development stages, depicted in Figure 3, illustrate the stepwise modifications made to achieve wideband performance and circular polarization.

**TABLE 1**. Antenna development stages.

| **Parameter** | **a** | **b** | **c** | **d** | **e** | **f** | **g** |
|---|---|---|---|---|---|---|---|
| Value (mm) | 30 | 25 | 5 | 11 | 0.5 | 9 | 0.5 |
| **Parameter** | **h** | **i** | **j** | **k** | **l** | **m** | **n** |
| Value (mm) | 1.5 | 11 | 6 | 7 | 8 | 5.5 | 4.5 |

The $S_{11}$ parameters at different stages of antenna development, as shown in Figure 4, demonstrate the progressive enhancement in impedance bandwidth. The initial design with an octagonal patch and full ground plane exhibited a narrow bandwidth, limiting its suitability for wideband applications. By modifying the patch into an octagonal ring and adopting a partial ground plane, a noticeable improvement in bandwidth was achieved. Further enhancements, including the addition of an inner octagonal patch, a hybrid slot, and a stub, optimized impedance matching across the 2.6–4.7 GHz range.

## 3. RESULTS AND DISCUSSIONS

The frequency vs. gain plot in Figure 5 illustrates the gain variation across the operating band, demonstrating stable perfor-

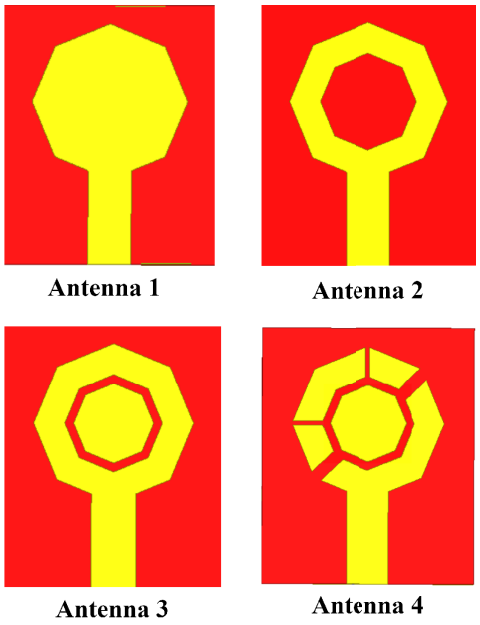


**FIGURE 3**. Antenna development stages.

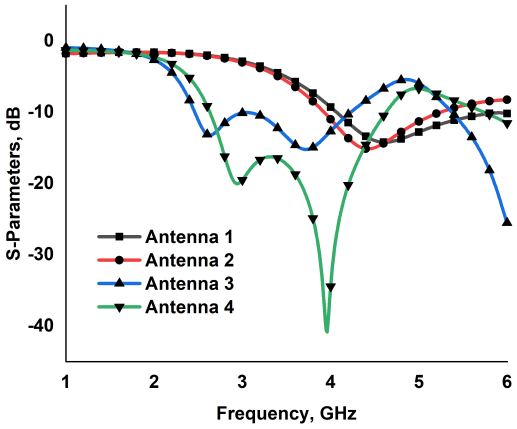


**FIGURE 4**. Return loss at antenna development stages.

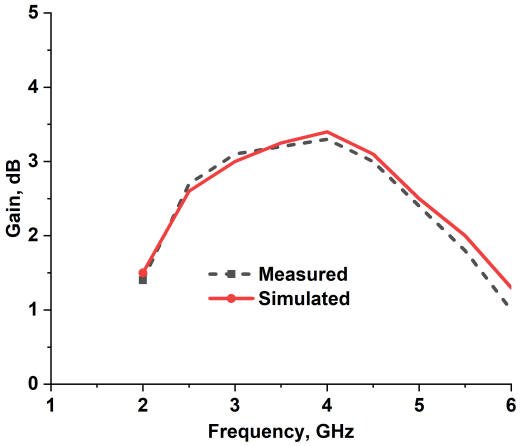


**FIGURE 5**. Gain of wideband antenna.

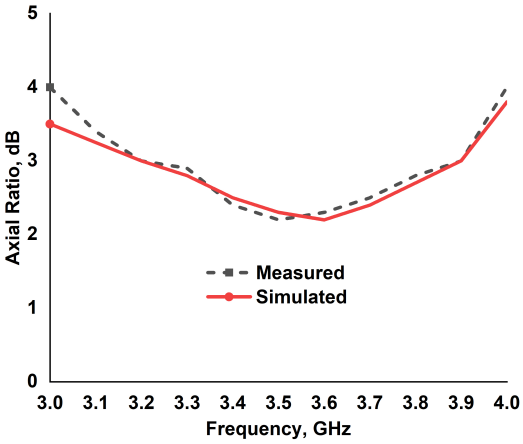


**FIGURE 6**. Axial ratio of wideband antenna.

mance between 2.6 GHz and 4.7 GHz. The antenna maintains a gain of 2.8–3.4 dB, ensuring reliable signal transmission for wearable applications. The slight variations in gain across the band are attributed to impedance matching and radiation efficiency enhancements introduced in the design.

The frequency vs. axial ratio plot in Figure 6 confirms the circular polarization characteristics of the antenna. The axial ratio remains below 3 dB between 3.2 GHz and 3.9 GHz, indicating effective circular polarization in this range. This polarization behaviour is achieved through the incorporation of four symmetrical slots in the ring patch, which generate orthogonal current components. The results validate the antenna's suitability for applications requiring polarization diversity and improved signal stability in dynamic wearable environments.

The $E$-plane and $H$-plane radiation patterns of the proposed antenna were analyzed at two intermediate operating frequencies, 2.92 GHz and 3.95 GHz as shown in Figure 7. As observed, the $E$-plane radiation pattern exhibits a figure-of-eight shape at both frequencies, which is characteristic of linearly polarized antennas and indicates good directivity. In contrast, the $H$-plane radiation pattern remains omnidirectional at both frequencies, ensuring uniform radiation in all directions. This omnidirectional behavior in the $H$-plane is beneficial for wearable applications, as it provides stable connectivity regardless of antenna orientation. These radiation characteristics confirm that the proposed antenna achieves a balanced trade-off between directionality and coverage, making it well-suited for body-centric wireless communication systems.

The electric field distribution on the patch at 2.92 GHz and 3.95 GHz is analyzed to understand the current flow and resonance behavior as shown in Figure 8. At 2.92 GHz, the field distribution shows strong excitation around the ring patch and feed line, indicating efficient radiation and impedance matching. At 3.95 GHz, the electric field is more concentrated around the slots and patch edges in one side of the patch. The observed field distributions confirm the effectiveness of the design modifications in achieving wideband operating frequency range.

The proposed antenna achieves CP through the generation of two orthogonal surface current components of equal magnitude with a 90° phase difference. Initially, an octagonal patch with a microstrip feed and full ground plane exhibited linear polarization with narrow impedance bandwidth. To improve impedance matching and enable polarization control, the struc-

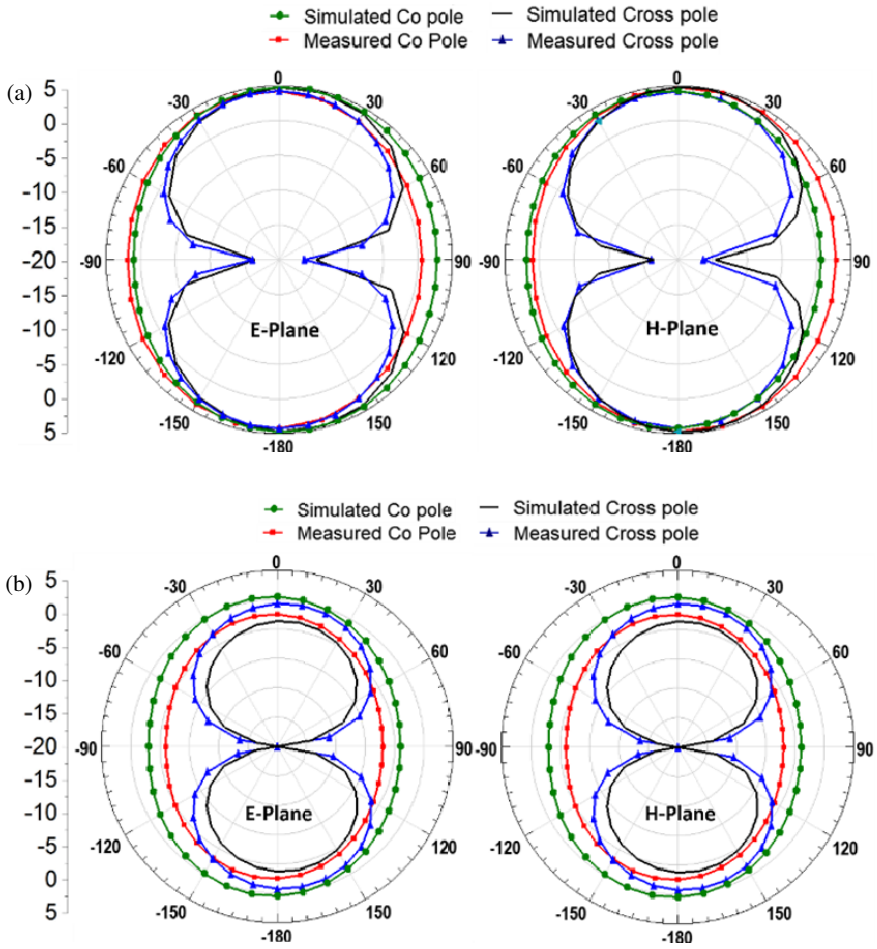


**FIGURE 7**. $E$ plane and $H$ plane patterns of wideband antenna, (a) at 2.92 GHz, (b) at 3.95 GHz.

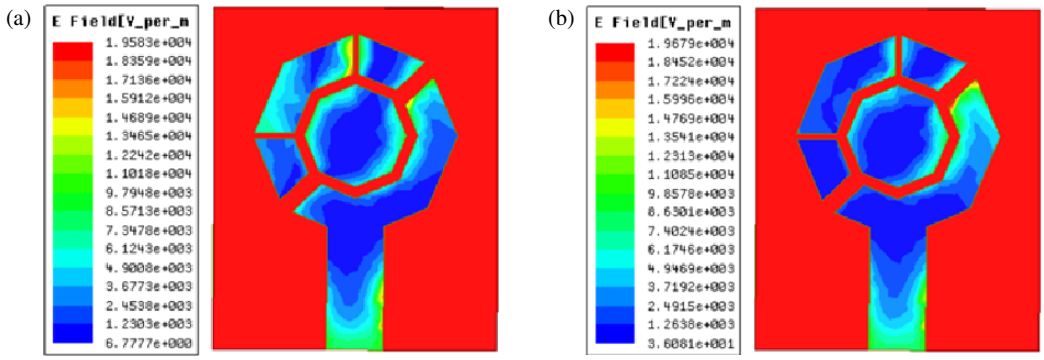


**FIGURE 8**. Electric field distribution of wideband antenna, (a) at 2.92 GHz, (b) at 3.95 GHz.

ture was modified into an octagonal ring patch and integrated with a partial ground plane containing a hybrid slot and stub. These modifications not only broadened the impedance bandwidth but also enhanced current coupling between the patch and ground.

To realize circular polarization, four symmetrical slots were etched along the edges of the octagonal ring patch. These perturbations effectively disturbed the current symmetry on the patch, thereby exciting two orthogonal modes ($TM_{01}$ and $TM_{10}$) with a quadrature phase relationship. The resultant superposition of these orthogonal modes produced circular polarization within the axial ratio (AR) bandwidth of 3.2–3.9 GHz.

The surface current distribution plots at 3.5 GHz as shown in Figure 9 confirm the rotational behavior of the current vectors in successive phase intervals, validating the generation of CP radiation. Furthermore, the simulated and measured axial-ratio responses show AR $< 3$ dB across the CP band, ensuring stable polarization characteristics. These results confirm that the combination of the ring geometry, ground perturbation, and

**TABLE 2**. Comparison of the proposed antenna.

| Ref. | Size ($\lambda^3$) | Bandwidth % | Gain (dB) | Axial Ration Bandwidth % |
|---|---|---|---|---|
| [5] | $0.76\lambda \times 0.76\lambda \times 0.04\lambda$ | 37.5 | 8.9 | 21.31 |
| [6] | $0.43\lambda \times 0.48\lambda \times 0.0081\lambda$ | 64.40 | 5.1 | 55.17 |
| [17] | $0.55\lambda \times 0.53\lambda \times 0.035\lambda$ | 42.6 | 3.5 | NA |
| [18] | $0.69\lambda \times 0.52\lambda \times 0.0047\lambda$ | 57.69 | 3.48 | NA |
| Proposed Work | $0.25\ \lambda \times 0.30\lambda \times 0.014\lambda$ | 57.5 | 3.4 | 19.7 |

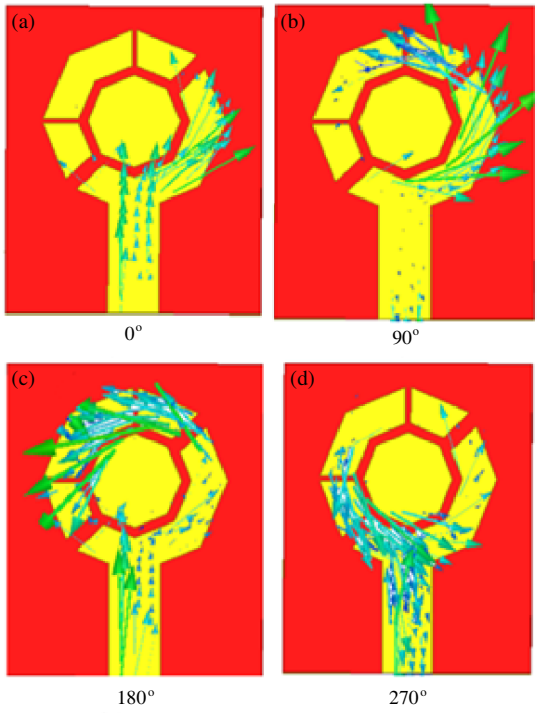


**FIGURE 9**. Surface current distribution at 3.5 GHz for different phase angles.

slot symmetry collectively facilitates circular polarization in the proposed design. Figure 10 shows the $S_{11}$ measurement setup.

For on-body simulation, a three-layer phantom model consisting of skin, fat, and muscle was used to evaluate the antenna's performance. Two analyses were conducted: SAR (Specific Absorption Rate) analysis and conformal analysis. The Specific Absorption Rate (SAR) quantifies the rate at which electromagnetic energy is absorbed per unit mass of human tissue when exposed to the antenna's near-field radiation. It is mathematically expressed as:

$$\text{SAR} = \frac{\sigma \mid E \mid^2}{2\rho} \tag{1}$$

where $\sigma$ is the electrical conductivity of the tissue (S/m), $\mid E \mid$ the magnitude of the induced electric field (V/m), and $\rho$ the mass density of the tissue (kg/m$^3$). SAR serves as a critical safety metric for wearable and biomedical antennas, ensuring that the electromagnetic exposure levels remain within the prescribed international standards (FCC: 1.6 W/kg over 1 g, ICNIRP/EU: 2 W/kg over 10 g of tissue).

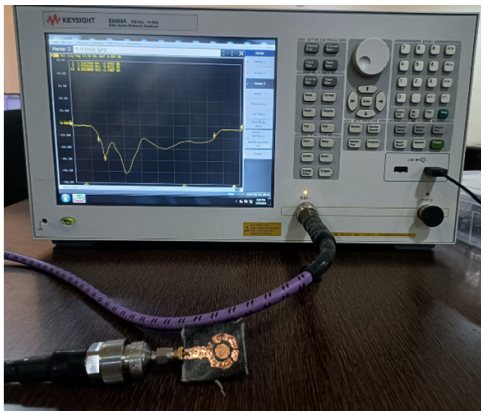

**FIGURE 10**. Antenna $S_{11}$ measurement.

In this work, SAR analysis was performed using a multilayer human tissue phantom consisting of skin, fat, and muscle layers as shown in Figure 11(a). The simulations were carried out to evaluate the antenna's behavior under realistic on-body conditions as shown in Figures 11(b) and 11(c). The SAR variation with frequency was obtained across the operational band of 2.6–4.7 GHz. It was observed that SAR values were higher at lower frequencies due to stronger near-field coupling and deeper field penetration into the tissue, whereas at higher frequencies, energy absorption was confined more superficially, resulting in reduced SAR levels as depicted in Figure 11(d).

Bending is an inevitable condition for wearable antennas, as they are typically integrated into garments or directly placed on curved parts of the human body. When an antenna is bent, the physical deformation alters the surface current distribution, effective electrical length, and coupling between the radiating patch and the ground plane, which can potentially shift the resonant frequency or degrade impedance matching. Therefore, bending analysis is essential to ensure stable performance under realistic wearable scenarios.

In the proposed design, the antenna was analyzed under cylindrical bending conditions to emulate typical curvatures of the human arm. The conformal evaluations were performed by wrapping the antenna on a multilayer phantom consisting of skin, fat, and muscle tissues, with curvature radii comparable to practical wearable cases as depicted in Figure 11(e). The return loss comparison among three configurations, antenna alone, antenna placed on a flat phantom, and antenna on a cylindrical phantom demonstrated negligible frequency shift and maintained $S_{11} < -10$ dB across the operational band, confirming mechanical robustness and electromagnetic stability as shown

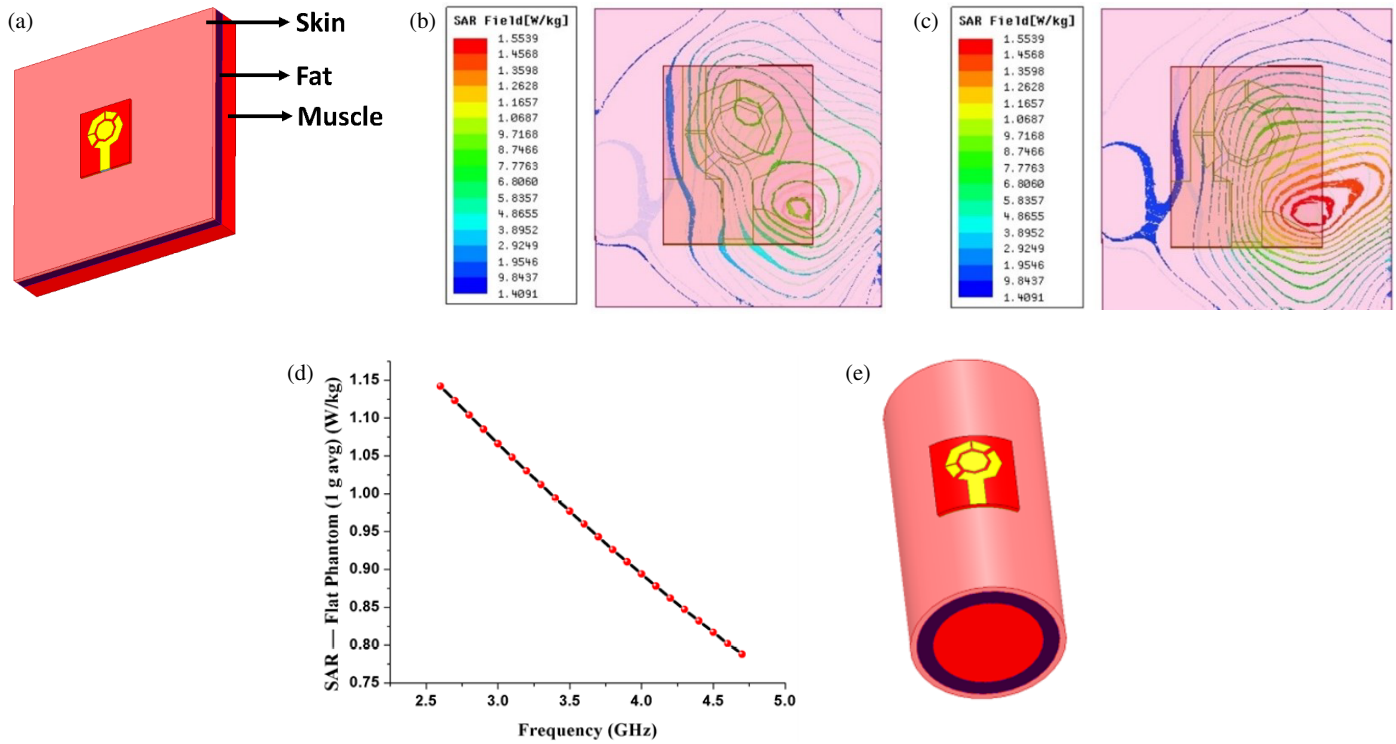


**FIGURE 11**. SAR and conformal analysis of antenna. (a) Antenna on rectangular phantom model. (b) SAR at 2.92 GHz. (c) SAR at 3.95 GHz. (d) Frequency vs specific absorption rate. (e) Antenna on cylindrical phantom model.

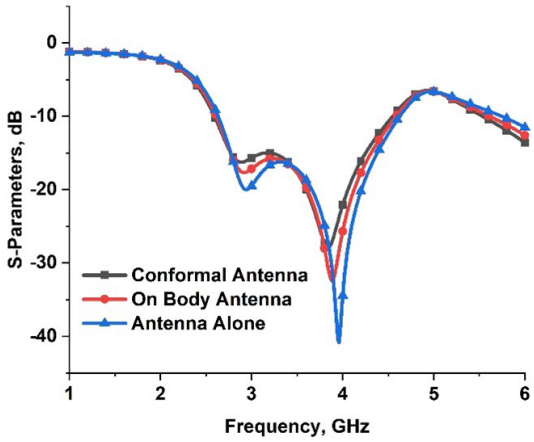


**FIGURE 12**. Return loss of wideband antenna.

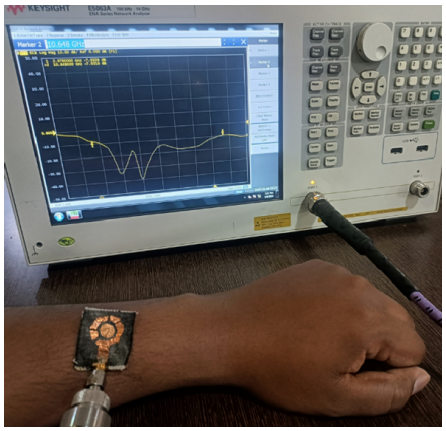

**FIGURE 13**. Antenna on body $S_{11}$ measurement.

in the Figure 12. Figure 13 presents the measurement setup for the on body measurement of the antenna.

Table 2 presents the comparison of the proposed antenna with earlier reported antennas.

## 4. CONCLUSION

A wideband circularly polarized wearable antenna operating from 2.6 GHz to 4.7 GHz was designed, fabricated, and analyzed. The antenna achieves circular polarization (3.2–3.9 GHz) with a stable gain of 2.8–3.4 dB. Design modifications, including an octagonal ring patch, partial ground, and hybrid slot, enhanced bandwidth and impedance matching. Measured $S_{11}$ results closely match simulations, validating the design. SAR analysis, on-body, and conformal simulations confirm its suitability for wearable applications. The radiation patterns exhibit a figure-of-eight $E$-plane and omnidirectional $H$-plane, ensuring stable performance. This antenna offers a compact and efficient solution for wearable communications, with future scope for miniaturization and multi-band integration.

## REFERENCES

[1] Chaudhary, S., A. Agarwal, D. Mishra, and S. Shah, "A review on Green communication for wearable and implantable wireless body area networks," *Computer Networks*, Vol. 252, 110693, 2024.

[2] Singh, S., R. Mishra, A. Kapoor, and S. Singh, "A comprehensive review and analysis of the design aspects, structure, and applications of flexible wearable antennas," *Telecom*, Vol. 6, No. 1, 3, 2025.

[3] Karthikeyan, T. A., M. Nesasudha, S. Saranya, and B. Sharmila, "A review on fabrication and simulation methods of flexible wearable antenna for industrial tumor detection systems," *Journal of Industrial Information Integration*, Vol. 41, 100673, 2024.

[4] Douhi, S., A. Boumegnane, N. Chakhchaoui, A. Eddiai, O. Cherkaoui, and M. Mazroui, "A wideband flexible antenna utilizing PMMA/PVDF-HFP/PZT polymer composite film and silver-based conductive ink for wearable applications," *Polymers for Advanced Technologies*, Vol. 35, No. 9, e6575, 2024.

[5] Baudh, R. K., S. Sahu, M. S. Parihar, and V. D. Kumar, "A wideband circularly polarized all textile on body antenna for defense applications," *IEEE Transactions on Circuits and Systems II: Express Briefs*, Vol. 71, No. 2, 567–571, Feb. 2024.

[6] Baudh, R. K., M. Kumar, S. Sahu, M. S. Parihar, and D. Kumar, "A low-profile, wideband, circularly polarized, slotted, U-shaped textile antenna for W-BAN applications," *ETRI Journal*, Vol. 47, No. 4, 579–589, 2025.

[7] Baudh, R. K., S. Sahu, M. S. Parihar, *et al.*, "A compact wideband low-profile all textile on/off body antenna for satcom and defense applications," *International Journal of Communication Systems*, Vol. 37, No. 17, e5933, 2024.

[8] Varma, D. R., M. Murali, M. V. Krishna, and G. S. N. Raju, "Miniaturized novel textile antenna for biomedical applications," in *2023 2nd International Conference on Paradigm Shifts in Communications Embedded Systems, Machine Learning and Signal Processing (PCEMS)*, 1–6, Nagpur, India, 2023.

[9] Marterer, V., M. Radouchová, R. Soukup, S. Hipp, and T. Blecha, "Wearable textile antennas: Investigation on material variants, fabrication methods, design and application," *Fashion and Textiles*, Vol. 11, No. 1, 9, 2024.

[10] Abdulla, F. A. A. and A. Demirkol, "A novel textile-based UWB patch antenna for breast cancer imaging," *Physical and Engineering Sciences in Medicine*, Vol. 47, No. 3, 851–861, 2024.

[11] Ibrahim, N. F., P. A. Dzabletey, H. Kim, and J.-Y. Chung, "An all-textile dual-band antenna for BLE and LoRa wireless communications," *Electronics*, Vol. 10, No. 23, 2967, 2021.

[12] Parameswari, S. and C. Chitra, "Textile UWB antenna with metamaterial for healthcare monitoring," *International Journal of Antennas and Propagation*, Vol. 2021, No. 1, 5855626, 2021.

[13] Kareem, F. R., M. E. Atrash, A. A. Ibrahim, and M. A. Abdalla, "Dual-band all textile antenna with AMC for heartbeat monitor and pacemaker control applications," *International Journal of Microwave and Wireless Technologies*, Vol. 14, No. 9, 1206–1221, 2022.

[14] Venkatachalam, D., V. Jagadeesan, K. B. M. Ismail, M. A. Kumar, S. Mahalingam, and J. Kim, "Compact flexible planar antennas for biomedical applications: Insight into materials and systems design," *Bioengineering*, Vol. 10, No. 10, 1137, 2023.

[15] Sakulchat, S., A. Ruengwaree, V. Thongpool, and W. Naktong, "Low-cost flexible graphite monopole patch antenna for wireless communication applications," *Computers, Materials & Continua*, Vol. 71, No. 3, 6069–6088, 2022.

[16] Singh, S. and S. Verma, "SAR reduction and gain enhancement of compact wideband stub loaded monopole antenna backed with electromagnetic band gap array," *International Journal of RF and Microwave Computer-Aided Engineering*, Vol. 31, No. 10, e22813, 2021.

[17] Yadav, A., P. Singh, R. K. Verma, and V. K. Singh, "Design and comparative analysis of circuit theory model-based slot-loaded printed rectangular monopole antenna for UWB applications with notch band," *International Journal of Communication Systems*, Vol. 36, No. 3, e5390, 2023.

[18] Jabbar, A., M. Zubair, M. A. Naveed, M. Q. Mehmood, and Y. Massoud, "A photopaper-based low-cost, wideband wearable antenna for wireless body area network applications," *IET Microwaves, Antennas & Propagation*, Vol. 16, No. 15, 962–970, 2022.